

## Supplementary Information

### **Optical Control of Ferroelectric Switching and Multifunctional Devices Based on van der Waals Ferroelectric Semiconductors**

Kai Xu<sup>1</sup>, Wei Jiang<sup>2</sup>, Xueshi Gao<sup>1</sup>, Zijing Zhao<sup>1</sup>, Tony Low<sup>2</sup> and Wenjuan Zhu<sup>1\*</sup>

*<sup>1</sup>Department of Electrical and Computer Engineering, University of Illinois at Urbana-Champaign, Urbana, Illinois 61801, USA*

*<sup>2</sup>Department of Electrical and Computer Engineering, University of Minnesota, Minneapolis, Minnesota 55455, USA*

## Characterization of $\alpha$ -phase $\text{In}_2\text{Se}_3$

Raman and photoluminescence (PL) spectra of an  $\text{In}_2\text{Se}_3$  flake are shown in Fig. S1a. Distinct Raman peaks at  $109\text{ cm}^{-1}$ ,  $186\text{ cm}^{-1}$ , and  $196\text{ cm}^{-1}$  correspond to the  $A_1(\text{LO}+\text{TO})$ , E and  $A_1(\text{TO})$  modes in  $\alpha$ -phase  $\text{In}_2\text{Se}_3$  respectively. The PL exhibits a peak of  $1.38\text{ eV}$ , which also indicates that the flake is  $\alpha$ -phase  $\text{In}_2\text{Se}_3$ . The inset of Fig. S1a illustrates the crystal structure of  $\alpha$ -phase  $\text{In}_2\text{Se}_3$ .

The ferroelectric properties of monolayer  $\text{In}_2\text{Se}_3$  cleaved from the bulk  $\alpha$ - $\text{In}_2\text{Se}_3$  were studied using density function theory (DFT) calculation. The plane-averaged local potential profile shows the potential drop of the vacuum level from the left to right side of the  $\text{In}_2\text{Se}_3$  (Fig. S1b), indicating existence of one intrinsic polarization within the  $\text{In}_2\text{Se}_3$  quintuple layers. This is consistent with a dipole moment of around  $-0.9\text{ e} \cdot \text{\AA}$  along the out-of-plane direction in the absence of an external E-field, which is indicative of its ferroelectric nature. To understand the physical origin, we performed the Bader charge analysis to study the charge distribution of  $\text{In}_2\text{Se}_3$  (Fig. S1c). The result shows that each In atom donates around 0.9 electron and each Se atoms accept around 0.6 electron, which yield an accumulation of negative ( $-0.3\text{ e}$ ) and positive ( $+0.3\text{ e}$ ) charges for the  $\text{InSe}_2$  trilayer and  $\text{InSe}$  bilayer substructures, respectively. Therefore, the built-in dipole moment is pointing from the  $\text{InSe}_2$  trilayer to the  $\text{InSe}$  bilayer. The polarization switching realized under external field is accomplished by shifting the position of the middle Se layer.

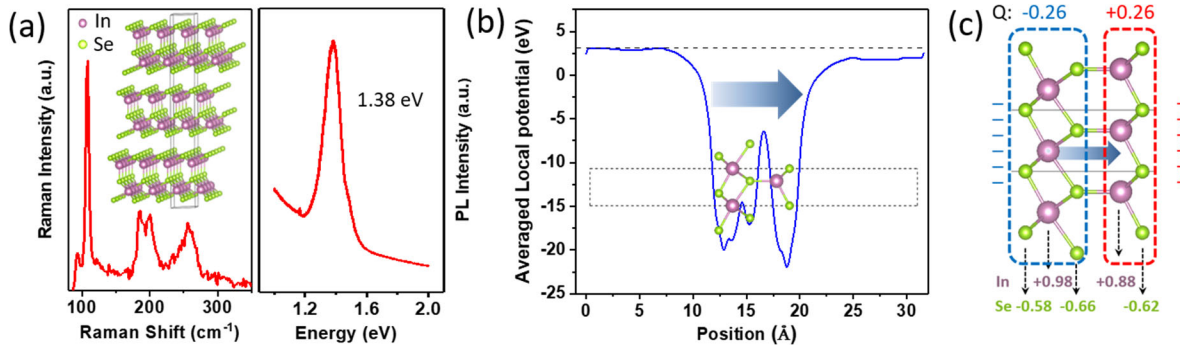


Figure S1. (a) Raman and photoluminescence spectra of an  $\text{In}_2\text{Se}_3$  flake. The inset of the Raman spectrum shows the crystal structure of  $\alpha$ - $\text{In}_2\text{Se}_3$ . (b) Averaged local potential profile for monolayer  $\text{In}_2\text{Se}_3$ . (c) Bader charge analysis shows the negative and positive charge accumulation at the trilayer ( $\text{InSe}_2$ ) and bilayer ( $\text{InSe}$ ), respectively. Positive and negative numbers represent loss and gain of electrons, respectively.

## Modelling of reversible Schottky diodes based on $\text{In}_2\text{Se}_3$

To gain insight into the charge transfer and band alignment in  $\text{In}_2\text{Se}_3$ /Graphene vdW heterostructure, DFT calculations based on bilayer graphene and  $\text{In}_2\text{Se}_3$  with two different polarization directions were studied. We plotted the atom-resolved projected band structure where graphene and  $\text{In}_2\text{Se}_3$  band can be clearly distinguished (Fig. S2). The graphene band shows an n-type and p-type doping with  $\text{In}_2\text{Se}_3$  polarization direction pointing to and away from the graphene, respectively.

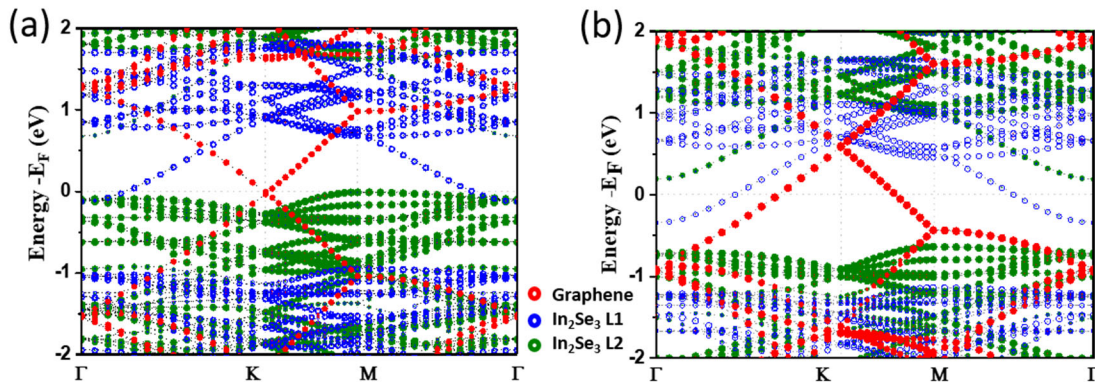


Figure S2. (a) and (b) Atom-resolved band structure for the  $\text{In}_2\text{Se}_3$ -graphene heterostructure. Red, blue, and green circles represent the contribution from graphene and two  $\text{In}_2\text{Se}_3$  layers, respectively.

## Memory window measurement

The setup for memory window measurement is illustrated in Fig. S3a. During the programming operation, the embedded gate is grounded and a voltage pulse is applied on the top gate. The source/drain terminals are floating during the programming operation. After each program pulse, a DC read operation is carried out. During the read operation, the source is grounded, the drain is biased at a constant voltage, and a DC voltage swept is applied on the embedded gate. The transfer curves measured after the positive and the negative program pulses are illustrated in Fig. S3b. The threshold voltage difference between these two transfer curves is defined as the memory window. Figure S2c shows the measured memory window as a function of program pulse amplitude for a dual-gate transistor with 21 nm thick  $\text{In}_2\text{Se}_3$ . We can see that the memory window is nearly zero when the program pulse amplitude is below 20 V and has a sharp increment when the program pulse amplitude exceeds 20 V. This step transition can be explained by the coercive voltage required for the polarization switching in  $\text{In}_2\text{Se}_3$ . In these memory window measurement, in order to minimize the impact of mobile ions, interface traps and bulk traps, we took several precautions. Low temperature is used to reduce the influence of the mobile ions and bulk traps on the threshold voltage shift. After program pulses, the gate voltage is returned to zero and no voltage is applied for a few minutes before the read operation starts. This will allow the interface trapped charges to have sufficient time to be released and has minimal impact on the threshold voltage. Furthermore, the read voltage applied on the embedded gate is very low to minimize the disturbance of the device during the read operation.

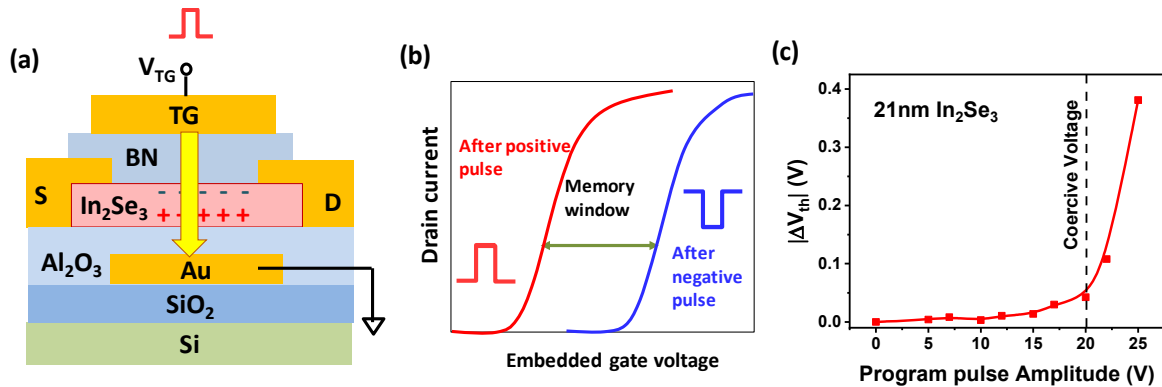


Figure S3. Measurement of memory window of  $\text{In}_2\text{Se}_3$  transistors. (a) Illustration of the measurement. During the programming operation, a pulse is applied on the top gate while the embedded gate is grounded. (b) Illustration of the transfer curves measured after a positive and a negative program pulses. The memory window is defined as the threshold voltage difference between these two transfer curves. (c) The measured memory window as a function of program pulse amplitude for a dual-gate  $\text{In}_2\text{Se}_3$  transistor. Here the threshold voltage shift is defined as  $|\Delta V_{th}| = |V_{th,p} - V_{th0}|$ , where  $V_{th,p}$  is the threshold voltage after the program pulse, and  $V_{th0}$  is the threshold voltage before the program pulse.  $|\Delta V_{th}|$  corresponds to approximately half of the memory window.

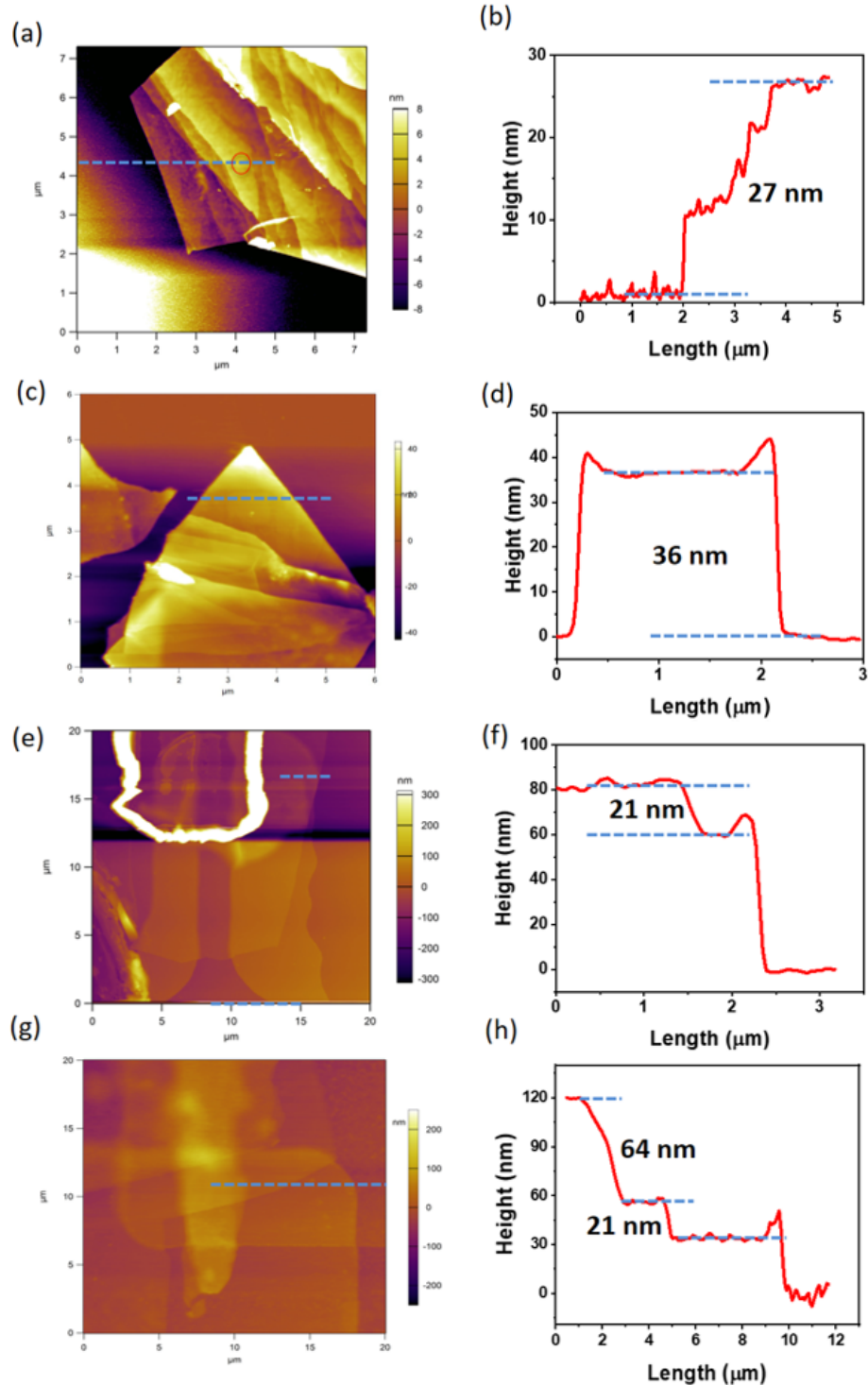


Figure S4. AFM images for (a) flake in Fig. 1a, (c) flake in Fig. 1b and 1c, (e) the device in Fig. 2c, and (g) the device in Fig. 4. The height profiles for these four cases are shown in (b), (d), (f) and (h) respectively. The thicknesses of the  $\text{In}_2\text{Se}_3$  are about 27 nm, 36 nm, 21 nm, and 64 nm for these four cases, respectively.

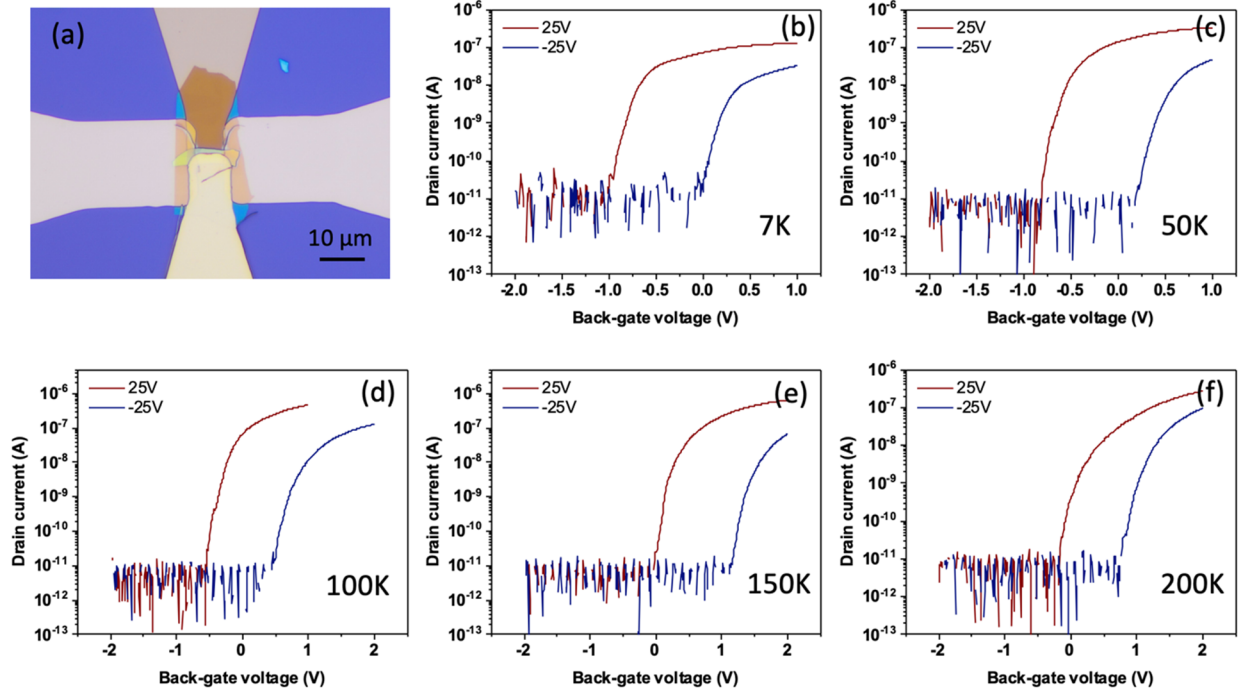


Figure S5. (a) Optical image and (b)-(f) temperature-dependent transfer curves of another  $\text{In}_2\text{Se}_3$  transistor with dual metal gates. This device shows ferroelectric tunability similar to that of the device discussed in the main text, further demonstrating the repeatability and stability of a ferroelectric  $\text{In}_2\text{Se}_3$  memory device.

## Electrostatics analysis of the dual-gate In<sub>2</sub>Se<sub>3</sub> memory device

To solve the charge distribution of the metal/insulator/ferroelectric vdW semiconductor, we assume the system to be charge neutral; i.e., the polarization charge ( $Q_{FE}$ ) is fully compensated by the induced charge in metal ( $Q_m$ ) and ferroelectric semiconductor itself ( $Q_{se}$ ),  $Q_m + Q_{se} = Q_{fe}$ . Considering an initial guess potential  $V_n$  of layer  $n$ , the voltage of layer  $n-1$  can be derived as  $V_{n-1} = -\frac{dQ_n}{\epsilon} + V_n$ , where  $d$  is the interlayer distance,  $\epsilon$  is the dielectric constant, and  $Q_n = \sum_{i=1}^n q_i$  is the cumulative charge up to the  $n$ th layer. The value of  $q_i$  can be calculated from  $q_i = \sum_j \frac{mgq_e k_B T}{\pi \hbar^2} \ln[1 + \exp(\frac{E_F - E_C^j}{k_B T})]$ , where  $m$  represent the effective mass of In<sub>2</sub>Se<sub>3</sub>,  $g$  is the valley degeneracy factor,  $q_e$  is the elementary charge,  $E_F$  is the Fermi-level energy, and  $E_C^j$  is the energy of the conduction band edge at the  $j$ th layer. The valley degeneracy factor is 1 for electrons, since the minimum of the conduction band is located at the Gamma valley in In<sub>2</sub>Se<sub>3</sub>. With the charge distribution, the potential profile can be calculated using Poisson's equation  $\nabla^2 \phi = -\rho/\epsilon$ . The cumulative voltage change will be the work function difference between metal and ferroelectric materials.

## Modeling of polarization charge and carrier charge density

To understand the relationship between pulse voltage and the charge density, we first analyzed the threshold voltage data with different pulse voltages. From the threshold voltage shift, we can derive the change of the charge density near the metallic surface based on the formula  $\Delta Q_m = \Delta V_{th} \cdot C_{ox}$ , where  $\Delta V_{th}$  is the threshold voltage shift and  $C_{ox}$  is the oxide capacitance. Here  $\Delta V_{th} = [V_{th}(+V_p) + V_{th}(-V_p)]/2$ , where  $V_{th}(+V_p)$  and  $V_{th}(-V_p)$  are the threshold voltages after positive and negative program pulses respectively. Because of the work function difference between metal (Au, 5.1 eV) and ferroelectric semiconductor (In<sub>2</sub>Se<sub>3</sub>, 4.35eV), there exists an initial charge density ( $Q_{m0}$ ) on the metal electrode. This can be solved using the electrostatic model without adding any polarization and with the work function difference included. Therefore, the total charge density near the metallic surface is  $Q_m = \Delta Q_m + Q_{m0}$ . The experimental data points of  $Q_m$  as a function of program pulse voltage were fitted using two error functions  $erf(x) = \frac{2}{\sqrt{\pi}} \int_0^x e^{-u^2} du$  to interpolate and extrapolate over range of pulse voltages of interest. Further, the polarization charge ( $Q_{FE}$ ) and free carrier charge density ( $q_i$ ) in In<sub>2</sub>Se<sub>3</sub> can be calculated from  $\Delta Q_m$  based on the aforementioned electrostatic analysis model.

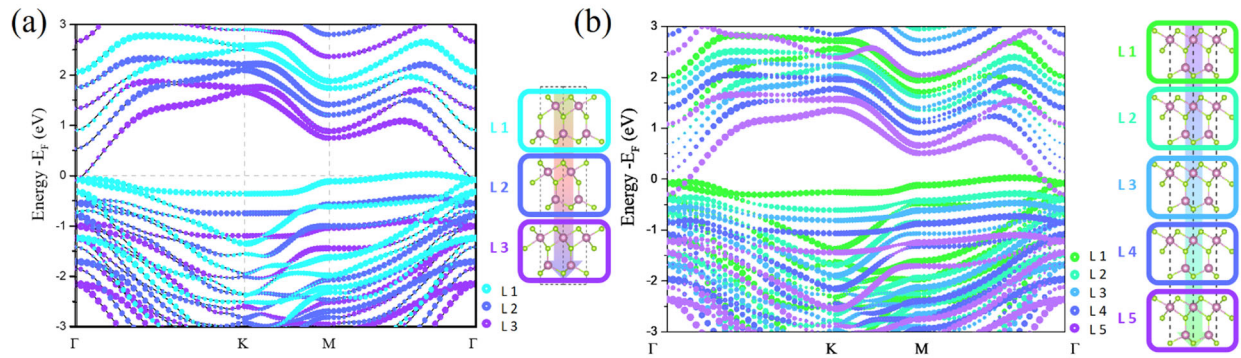


Figure S6. Layer-resolved band structure. (a) Band structure contributed from different layers in three-layered  $\text{In}_2\text{Se}_3$ . (b) Same as (a) for five-layered  $\text{In}_2\text{Se}_3$ . Band structure from each  $\text{In}_2\text{Se}_3$  layer is labelled with a unique color. Clearly shown along the dipole direction is that the band structure shifts downward to the lower energy, which is also consistent with plane-average potential profile that drops along the dipole direction. It is worth mentioning that with the increase of the layer thickness, the built-in electric field essentially decreases as the total potential drop across the system becomes constant.



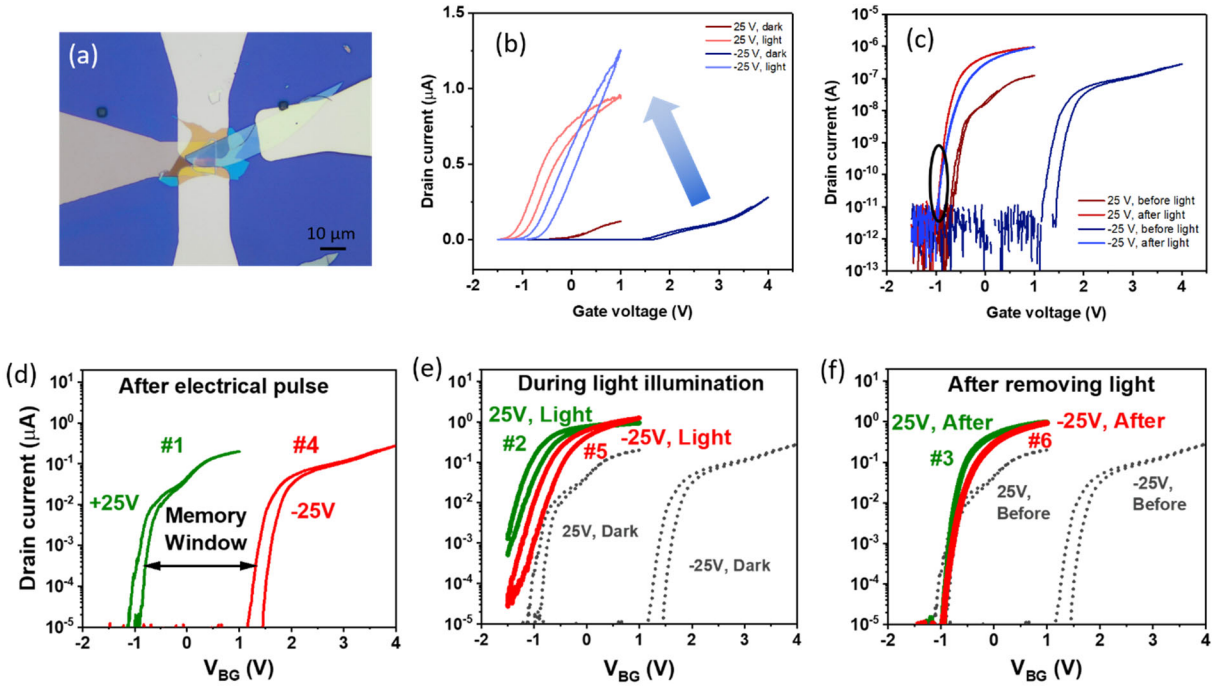


Figure S7. Other multifunctional  $\text{In}_2\text{Se}_3$  device with transparent electrodes. (a) Optical image of the device. (b) Photoresponse after +25 V and -25 V program pulses. (c) The transfer curves before light illumination and after light removal. (d)-(f) Transfer curves of another  $\text{In}_2\text{Se}_3$  device after electrical pulse, during light illumination and after removing light. The results also exhibit photo-induced polarization switching, indicating that this effect is repeatable and reliable.

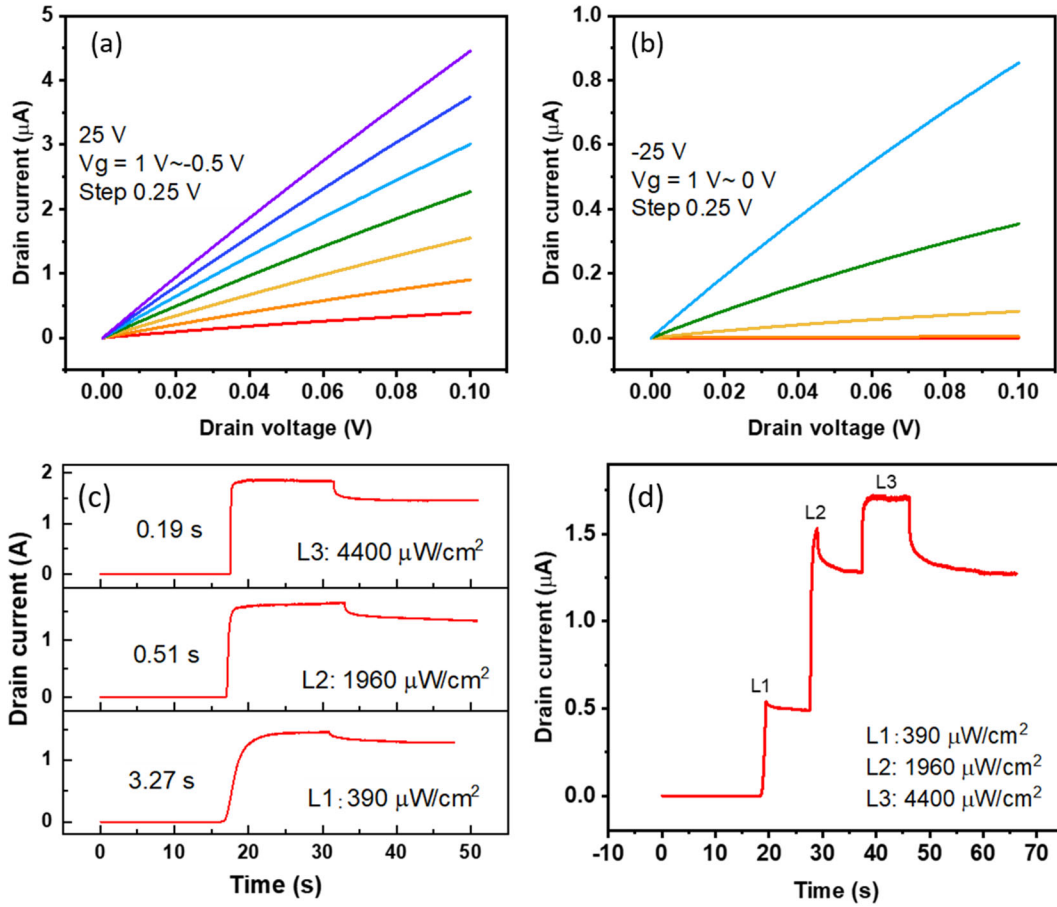


Figure S8. The output curves of  $\text{In}_2\text{Se}_3$  memory device with graphene electrode after  $+25\text{ V}$  (a) and  $-25\text{ V}$  (b) pulses. (c) and (d) Time evolution of drain current after  $-25\text{ V}$  pulse and then illuminated with light with three different intensities. It took longer time for the light with low intensity to flip the ferroelectric polarization completely.